International Symposium
On Turbulence and Shear Flow
Phenomena (TSFP-8)
August 28 - 30, 2013 Poitiers, France

STABILIZATION OF SUBCRITICAL BYPASS TRANSITION IN THE LEADING-EDGE BOUNDARY LAYER BY SUCTION

Michael O. John
Institute of Fluid Dynamics
ETH Zurich
8092 Zurich, Switzerland
john@ifd.mavt.ethz.ch

Dominik Obrist
Institute of Fluid Dynamics
ETH Zurich
8092 Zurich, Switzerland
obrist@ifd.mavt.ethz.ch

Leonhard Kleiser
Institute of Fluid Dynamics
ETH Zurich
8092 Zurich, Switzerland
kleiser@ifd.mavt.ethz.ch

ABSTRACT

This work investigates the subcritical transition in the swept Hiemenz boundary layer (SHBL) by means of direct numerical simulations (DNS). A combination of a steady and a time-dependent disturbance leads to spatial bypass transition. The primary disturbance consists of steady co-rotating vortices, leading to streaks. The secondary, time-dependent disturbance interacts with the streaks and instability and breakdown may occur. The instability is strictly of secondary nature and only occurs for a certain band of secondary disturbance frequencies.
The influence of uniform suction across the wall on this bypass transition is investigated. Analogous to results from linear stability theory, also the secondary stability is enhanced by suction. Depending on the Reynolds number and the suction strength, the unstable disturbances are shown to be either localized structures, convected along the streamlines, or global structures, covering broad regions in the downstream direction.

INTRODUCTION

The SHBL is found on a flat plate when the far-field consists of a plane impingement flow (Hiemenz, 1911) and an additional perpendicular sweep velocity component. It has found wide application as a model for the flow along the attachment line of swept airplane wings. The Reynolds number of the problem is defined as $Re = W_\infty/\sqrt{a\nu}$, where W_∞ is the sweep velocity of the far-field, a the rate of strain of the impingement flow, ν the kinematic viscosity.
Solutions for the linear stability of the three-dimensional flow were formulated by Görtler (1955) and Hämmerlin (1955), while Pfenninger (1977) and Poll (1979) found it to be subcritically unstable with a linear critical Reynolds number of $Re_c = 583.1$. The global critical Reynolds number, below which no disturbance can lead to transition, was estimated as $Re_{c,gl} \approx 250$.
Hall *et al.* (1984) investigated the linear stability problem under application of suction at the wall. The corresponding non-dimensional parameter is $\kappa = V_0/\sqrt{\nu a}$, where $-V_0$ is the suction velocity. They showed that the linear critical Reynolds number is substantially increased if suction is applied. Further extensions to weakly nonlinear theory were performed (Hall & Malik, 1986) and numerical simulations with suction were carried out by Joslin (1995), but only for small values of κ and in the vicinity of the linear critical value for Re. To date, no theoretical explanation of the experimental value for $Re_{c,gl}$ is known and the influence of suction on the subcritical transition needs clarification.
Recently, a nonlinear subcritical spatial transition mechanism was reported by Obrist *et al.* (2012), the cornerstone of which is the interaction of a pair of steady streamwise vortices with an unsteady, secondary perturbation of much lower amplitude. The vortices were earlier identified as optimal disturbances with respect to the formation of streaks and transient energy growth (Guegan *et al.*, 2007). This bypass scenario closely resembles the transition known from two-dimensional flat plate boundary layers (Landahl, 1980; Waleffe, 1997). Transition in simulations of the flow around swept wings as a result of the interaction of steady with unsteady perturbations was as also reported by Hosseini *et al.* (2013).
In the remainder of the paper we explain the methodology of the DNS performed and provide information on the type of disturbances which initiate the instability. The results section first focuses on the influence that the primary and the secondary instabilities have on the disturbance energy. The secondary instability nature of the bypass transition scenario is investigated, i.e. the base flow is found to be stable with respect to the primary disturbance alone, even for relatively large amplitudes. We then present parametric dependencies of the secondary instability on the strength of the suction κ and the Reynolds number Re and we report on different transition locations. Finally, we present the conclusions.

METHODOLOGY

We perform DNS of the incompressible swept Hiemenz boundary layer flow using our in-house code

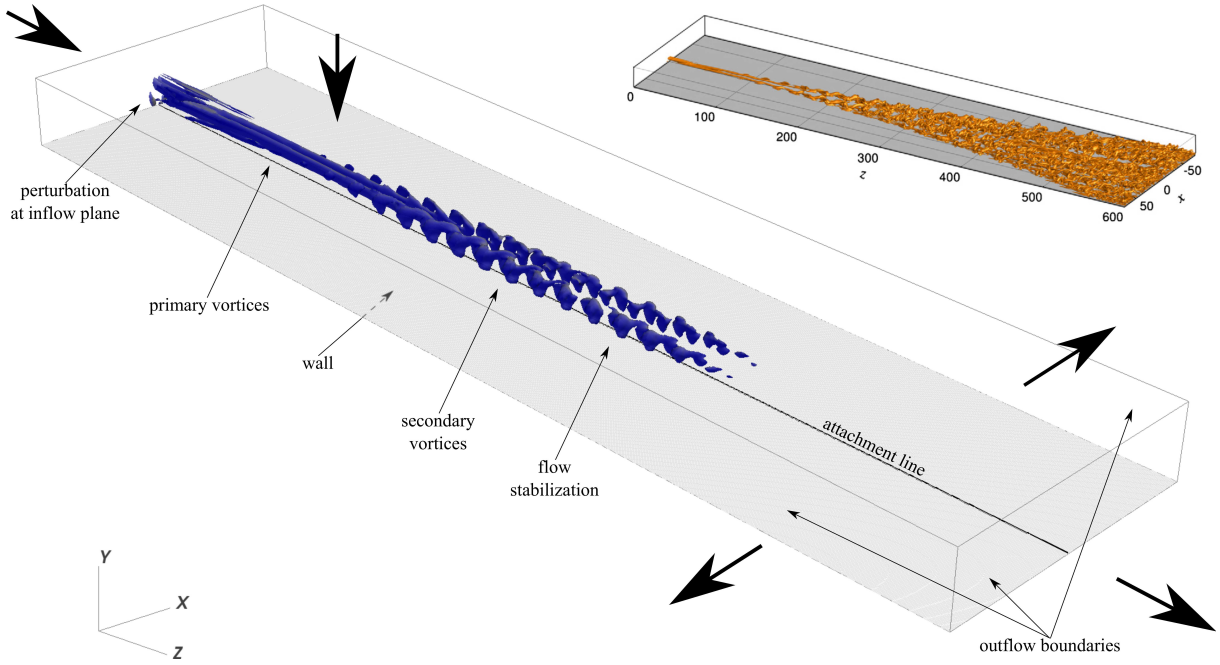

Figure 1. Typical isosurfaces $\lambda_2 = -10^{-3}$ of the λ_2 vortex criterion for a flow configuration stabilized by suction. The perturbation at the inflow plane $z = 0$ leads to the growth of primary and secondary vortices ($Re = 370$, $\kappa = 1.0$, $T_2 = 30$). Simulations at the (even lower) Reynolds number $Re = 300$ were found to be unstable (top right) with respect to an identical perturbation by Obrist *et al.* (2012).

IMPACT (Henniger *et al.*, 2010). The Navier-Stokes equations are discretized in all three spatial directions by sixth order finite differences on a structured Cartesian grid. The time-integration is semi-implicit (explicit Runge-Kutta for nonlinear terms/Crank-Nicolson for linear terms). Except for the wall suction and the shape of the spatial disturbances, the configuration of the simulations follows Obrist *et al.* (2012): The SHBL solution is initiated in the full computational domain. Spatial disturbances are prescribed at the inflow plane $z = 0$ and the exact SHBL solution is prescribed as Dirichlet conditions at the top inflow plane (cf. fig. 1). At the remaining three open boundaries we prescribe advective outflow conditions for the velocity disturbances (i.e. the deviation from the SHBL) in the direction normal to the boundary.

Primary and secondary disturbance

The spatial disturbances consist of a pair of counter-rotating vortices imposed at the inflow plane $z = 0$, aligned with the streamwise z direction, $\underline{u}'(x,y,z=0,t) = (u'(x,y,t), v'(x,y,t), 0)^T$. Their amplitude is chosen to oscillate around a steady mean, $\underline{u}'(x,y,t) = \vec{\underline{u}}'(x,y) \cdot [1 + A_2 \sin(2\pi t/T_2)]$. The maximum mean velocity amplitude $A_1 = \max_{x,y} |\vec{\underline{u}}'|$ and other parameters (e.g. geometrical position, radial extent) are prescribed for the generic pair of vortices, which give rise to streaks of streamwise velocity. We consider the arising streak velocity excess amplitude defined as

$$A_{St}(z) = \max_{x,y}(|w(x,y,z) - w_B(x,y)|)/W_\infty,$$

where w_B is the laminar SHBL base flow. Typical values of A_{St} for different primary vortex amplitudes A_1 are shown in figure 2.

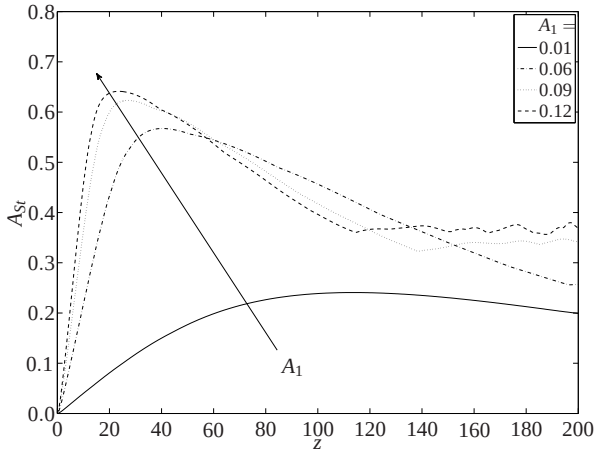

Figure 2. Maximum streak velocity excess as a function of streamwise position z and amplitude of the primary vortices A_1 for large times, $Re = 370$, $\kappa = 0.12$, $A_2 = 0.0012$

Measures of disturbance energy

In order to quantitatively describe the stability properties of the flows, two measures of the disturbance energy are employed. The first is the total disturbance energy

$$E(z,t) = \int_{-\infty}^{\infty} \int_{0}^{\infty} (\underline{u}(x,y,z,t) - \underline{u}_B(x,y))^2 \, \mathrm{d}y\mathrm{d}x,$$

where $\underline{u}_B$ is the SHBL base flow. $E(z,t)$ expresses the deviation of the flow from the laminar solution. The time-dependent function attains statistically stationary values for sufficiently large times.

In order to quantitatively assess the secondary instability

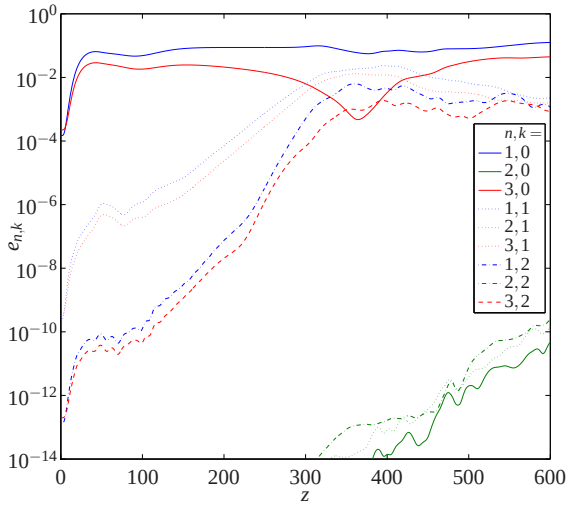

Figure 3. Typical Fourier-Hermite spectral energy density $e_{k,n}(z)$, showing initial primary modes (stationary $k = 0$, symmetric with respect to $x = 0$, n odd) and the growth of secondary ($k > 0$) modes. $Re = 370$, $\kappa = 0.6$, $T_2 = 30$, $A_1 = 0.10$

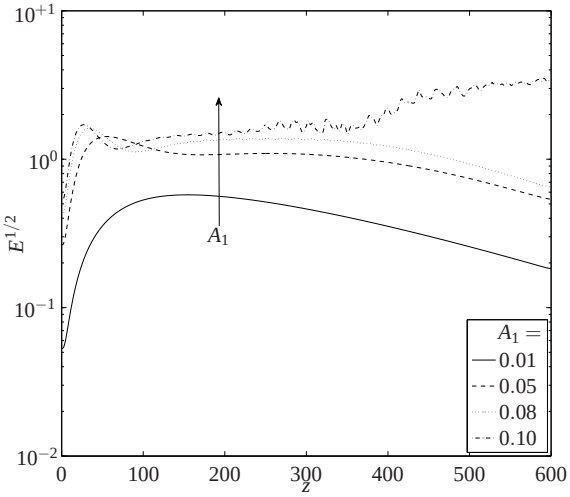

Figure 4. $E^{1/2}(z, t = 1500)$ for different primary disturbance amplitudes A_1 at $Re = 367.42$, $\kappa = 0.12$, $T_2 = 18.4$, $A_2 = 0.001$

and its growth rate a Fourier-Hermite spectral decomposition of the instantaneous flow is performed, which provides time-independent spectral disturbance energy densities

$$e_{k,n}(z) = \int_0^\infty |\hat{u}'_{k,n}(y,z)|^2 + |\hat{v}'_{k,n-1}(y,z)|^2 + |\hat{w}'_{k,n-1}(y,z)|^2 \, \mathrm{d}y$$

for the various modes, computed from

$$\underline{\hat{u}}'_{k,n}(y,z) = \int_{t_a}^{t_b} \int_{-\infty}^{\infty} \underline{u}'(x,y,z,t) \cdot \mathrm{He}_n(x) \cdot \mathrm{e}^{-(x/(\sqrt{2}\gamma))^2} \mathrm{d}x \cdot \mathrm{e}^{-i2\pi k t/T_2} \, \mathrm{d}t,$$

where $He_n(x)$ is the Hermite polynomial of order n and $\gamma = 10$ as a typical value (Obrist & Schmid, 2003). The starting point for the analysis $t_a \approx 1800$ is such that the simulations have attained a statistically stationary disturbance energy $E(z,t)$ and the time interval $t_b - t_a$ is set to contain approximately 10 to 20 periods of duration T_2.

RESULTS

A typical spectral decomposition of an unstable flow is shown in figure 3. The primary disturbance leads to non-zero stationary modes ($k = 0$), which are symmetric with respect to the center plane $x = 0$ (n odd). Secondary modes ($k = 1$) grow exponentially after a short transient period. These modes are still symmetric (n odd) with respect to $x = 0$. Only far downstream do even modes (n even) grow to substantial values, which eventually leads to fully developed turbulent flow.

The growth rate α of the secondary instability may be estimated from

$$e_{1,1}(z) \approx e_{1,1}(z = z_0) \cdot \mathrm{e}^{\alpha(z-z_0)}$$

for some suitable z_0, marking the position of the onset of modal growth of the secondary instability (e.g. $z_0 \approx 120$ in fig. 3). For almost all simulations robust positions z_0 could be identified, from where on exponential growth of $e_{1,1}$ could be observed.

Verification of secondary instability

With these measures we verified that the mentioned bypass transition scenario is in fact based on a secondary instability phenomenon. On the one hand, as long as the secondary amplitude A_2 is zero, no transition can be found, even though the energy of the pair of primary vortices is seen to increase by several orders of magnitude. For non-zero A_2, however, α shows a rather high sensitivity to the amplitude of the primary vortices (fig. 4). On the other hand, given a primary disturbance, α is found to be quasi independent of $A_2 > 0$. At the same time, a significant influence of the period of the secondary disturbance T_2 on α is observed. A band of unstable frequencies is found, with α attaining its maximum at approximately $T_2 \approx 15...20$ (fig. 5).

Influence of boundary suction κ and of Re

The subcritical instability described above may be stabilized by suction at the wall (fig. 1), i.e. a flow at a given Re, which would lead to transition through secondary instability in the absence of suction, may seen to be stabilized. This stabilization of the flow, however, is not entirely comparable to the well-known results of linear stability theory (Hall *et al.*, 1984), because it is an effect of the secondary stability. The energy contained in the primary disturbances, obtained transiently from the base flow, is not substantially reduced by suction and no (quasi-)monotonic energy decrease is observed. Rather, the primary disturbance energy remains of the same order of magnitude and only the growth rate α of the secondary disturbance is reduced. This effect may even completely stabilize the flow, if α becomes negative. In all cases, a reduction of α is achieved by increasing suction and transition is delayed to larger values of z. The ability of κ to alter the stability properties for a given base

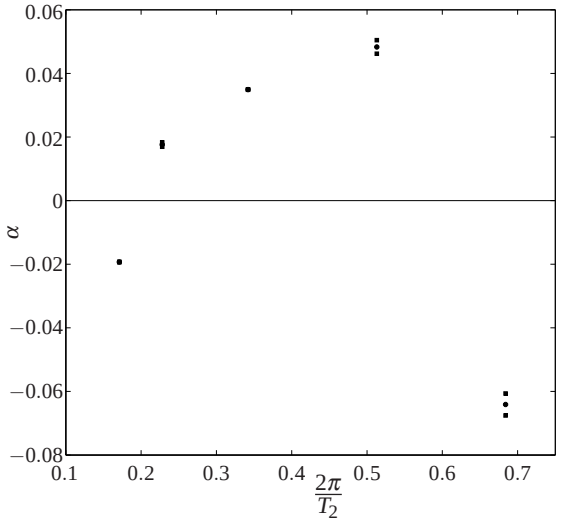

Figure 5. Secondary instability growth rate α (and standard deviations arising from different choices of z_0) as a function of the secondary disturbance period T_2 at $Re = 367.4$, $\kappa = 0.12$, $A_1 = 0.1155$

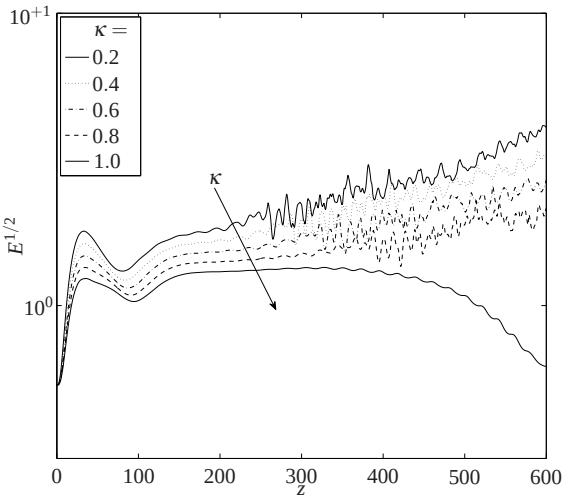

Figure 6. $E^{1/2}(z, t = 1500)$ for different values of κ at $Re = 370$, $T_2 = 30$, $A_1 = 0.10$

flow and disturbance is summarized in figure 6.

As in the case of linear stability theory, increasing Re leads to larger secondary instability growth rates α. Therefore, unstable flows undergo transition earlier. Figure 7 illustrates these effects.

Summarizing the results of the two preceding sections, figure 8 shows the growth rates α for the various simulations as a function of both Re and κ. It is interesting to compare the locations of the unstable simulations in the (Re, κ)-plane with that of the neutral curve of linear stability theory, denoted in the figure by the solid line. All simulations above and to the left of the neutral curve are linearly stable. Non-linearly unstable flows can be found even at large distances from the linear neutral curve, for very low values of Re (e.g. $Re = 300$ when $\kappa = 0$, as opposed to

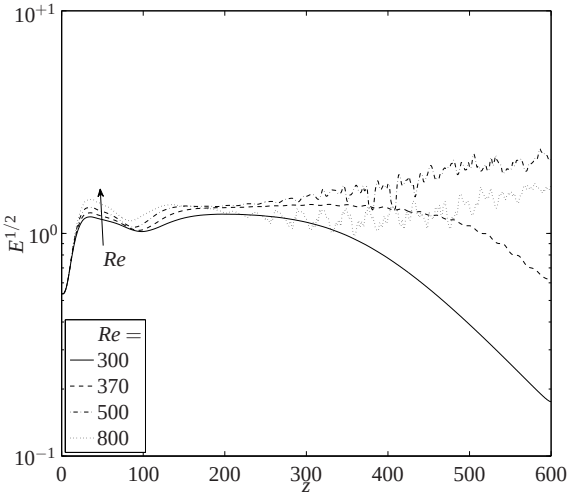

Figure 7. $E^{1/2}(z, t = 1500)$ for different values of Re at $\kappa = 1.0$, $T_2 = 30$, $A_1 = 0.10$

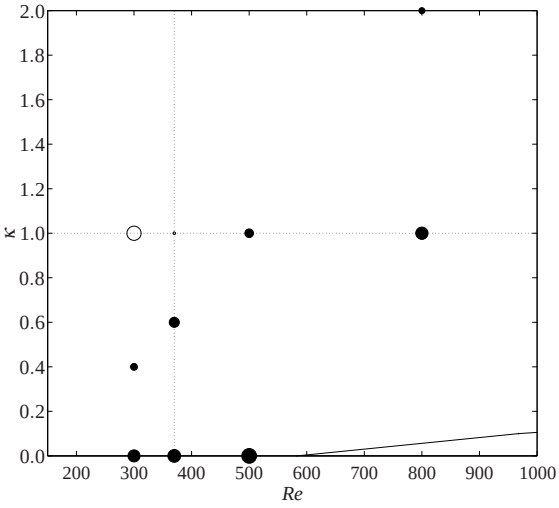

Figure 8. Growth rates α of the mode e_{11} as a function of Re and κ for $T_2 = 30$, $A_1 = 0.10$. The radii of the circles are proportional to α, solid circles denote positive (unstable) and open circles negative (stable) values. The solid line denotes the neutral curve of linear stability theory (Hall *et al.*, 1984). The dotted lines correspond to $\kappa = 1.0$ and $Re = 370$, respectively, which are the values taken for figures 6 and 7.

$Re_{c,lin}|_{\kappa=0} \approx 583.1$) and for very large values of κ (e.g. $\kappa = 2.0$ when $Re = 800$, as opposed to $\kappa_{c,lin}|_{Re=800} \approx 0.06$). This demonstrates the effectiveness of the combination of counter-rotating primary vortices as a primary disturbance and a weak unsteady secondary perturbation for triggering transition.

Despite the apparent effectiveness of the disturbance, even moderate values of κ suffice to stabilize the flow at $Re = 300$. This is consistent with the fact that $Re_{c,gl} \approx 250$ is the global critical limit, reported experimentally by Poll (1979), below which virtually no disturbance may destabilize the flow, even in the absence of suction.

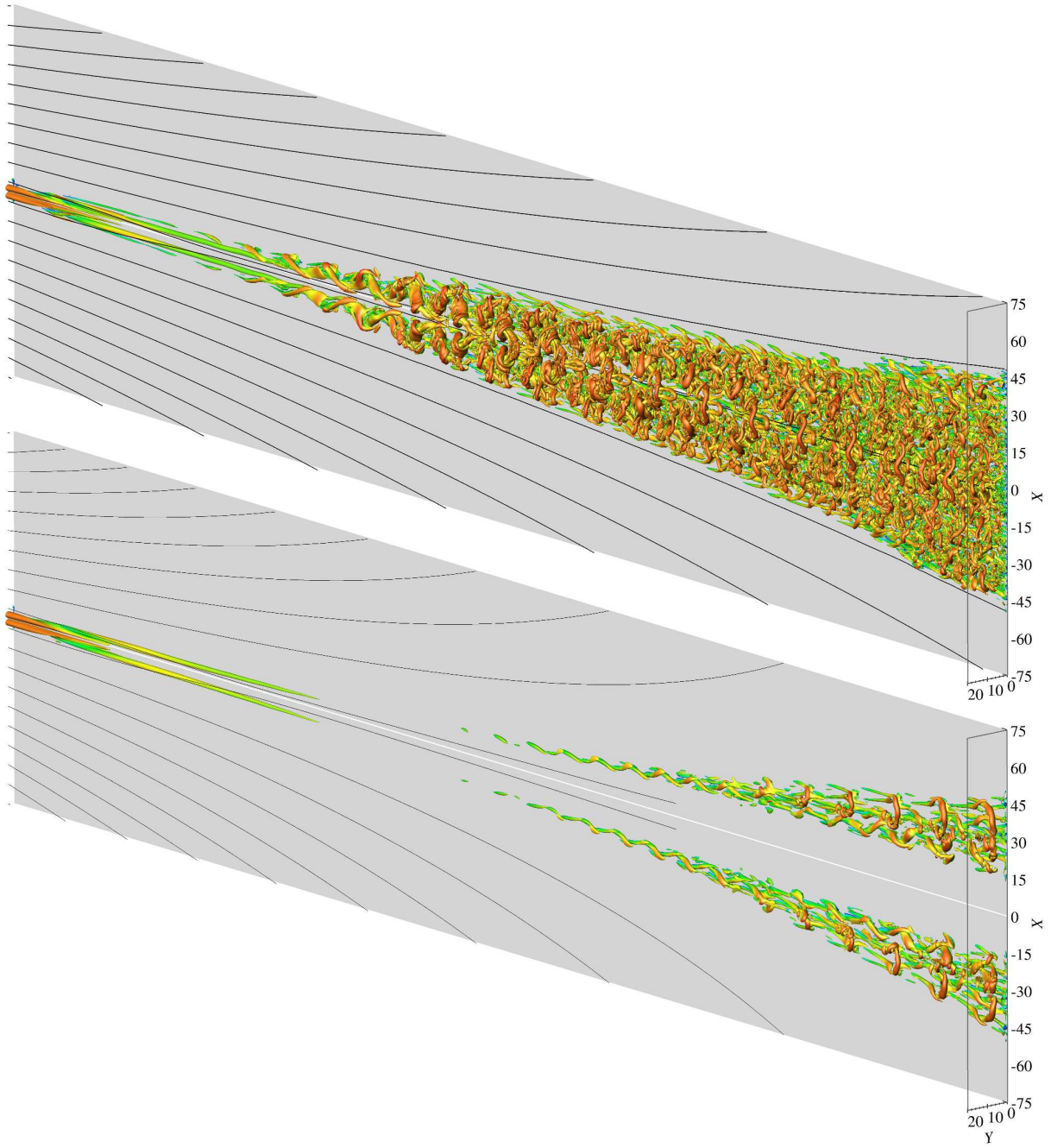

Figure 9. Visualization of transition by isosurfaces $\lambda_2 = -10^{-4}$ of the λ_2 vortex criterion. Top: $Re = 500$, $\kappa = 0.0$, $T_2 = 30$, $A_1 = 0.10$, bottom: $Re = 300$, $\kappa = 0.4$, $T_2 = 30$, $A_1 = 0.10$, both colored by the local streamwise velocity $w(x,y,z)$. The black lines are streamlines originating at $z = 0$ inside the boundary layer approximately at mid-depth $y = 1.5$.

Analogy to absolute/convective instability

Another interesting feature of the instability is the direction of its spatial evolution. For any given disturbance the combination of Re and κ defines not only the (secondary) growth rate of the instability of the flow, but also the geometric properties of the base flow. Especially, altering Re or κ alters the boundary layer thickness (i.e. the length scale of the boundary layer) and the rate of divergence of the streamlines of the base flow. Thus, both the instability and the geometrical evolution are simultaneously defined by Re and κ. For the inflow disturbance type used we observe three kinds of spatial evolution.
First, the flow may be stable and the secondary disturbances may be damped. In this case no transition is observed and far downstream the base flow is recovered (fig. 1). The second picture is that of spatial instability. In this case disturbances grow primarily in the z-direction (cf. fig. 9(a)). The transition region widens until the coherent structures break down. Finally, the region of turbulent flow covers an entire wedge-shaped area, confined by diverging streamlines of the laminar base flow. The contaminated region extends from a negative to a positive chordwise location, such that this kind of spatial evolution may be seen as the analog to "absolute instability" known from linear stability theory.
The third spatial transition scenario (fig. 9(b)) is distinctively different from the second. It is also unstable, but the disturbances are concentrated to within a small band, following the direction of the outer streamlines of the base

flow. Therefore, the disturbance growth is localized in space. For any spatial position (x,y) the laminar base flow is recovered at a sufficiently large value of z. This scenario may be understood as an analogy to "convective instability". One must thus bear in mind that measuring the growth rate α in the x or z direction alone is not sufficient for a physically sensible description of the transition, because two qualitatively different transition configurations may lead to identical growth rates α.

CONCLUSIONS

We have carried out simulations of the SHBL which exhibit bypass-transition of laminar to turbulent flow at subcritical Reynolds numbers. The flows were perturbed with a pair of counter-rotating vortices, leading to streaks. The streaks were seen to be destabilized by a secondary, time-dependent disturbance, which needs to lie within a certain frequency band. This combination of disturbances leads to a secondary instability of the base flow and proves very effective in generating turbulent flow. Even for Reynolds numbers much lower than the linear critical value, transition could be observed.

Application of suction at the wall was shown to reduce the growth rates of the secondary instability, i.e. to delay transition. This is understood as an extension of the results known from linear stability theory, where the application of suction is known to increase the linear critical Reynolds number. Large enough suction may even lead to flow stabilization. Nevertheless, for strong primary disturbances, subcritical instability was found even for very large suction values.

Changing Re and κ alters not only the secondary instability growth rates but also the length scale of the base flow and the rate of divergence of its streamlines. Therefore, a phenomenon analogous to convective and absolute instability was observed. If the flow is unstable, not only contamination of the entire leading edge could be observed, but also an entirely laminar flow sufficiently far downstream. Hence, knowledge of the growth rate of the secondary instability alone is not sufficient to predict the area where turbulent flow is to be expected.

REFERENCES

Görtler, H 1955 Dreidimensionale Instabilität der ebenen Staupunktströmung gegenüber wirbelartigen Störungen. In *50 Jahre Grenzschichtforschung. Eine Festschrift in Originalbeiträgen.* (ed. H Görtler & W Tollmien), pp. 304–314. Braunschweig: Vieweg.

Guegan, A, Huerre, P & Schmid, P J 2007 Optimal disturbances in swept Hiemenz flow. *Journal of Fluid Mechanics* **578**, 223–232.

Hall, P & Malik, M R 1986 On the Instability of a Three-Dimensional Attachment-Line Boundary-Layer: Weakly Nonlinear Theory and a Numerical Approach. *Journal of Fluid Mechanics* **163**, 257–282.

Hall, P, Malik, M R & Poll, D I A 1984 On the Stability of an Infinite Swept Attachment Line Boundary Layer. *Proceedings of the Royal Society of London Series A-Mathematical Physical and Engineering Sciences* **395** (1809), 229–245.

Hämmerlin, G 1955 Zur Instabilitätstheorie der ebenen Staupunktströmung. In *50 Jahre Grenzschichtforschung. Eine Festschrift in Originalbeiträgen* (ed. H Görtler & W Tollmien), pp. 315–327. Braunschweig: Vieweg.

Henniger, R, Obrist, D & Kleiser, L 2010 High-order accurate solution of the incompressible Navier-Stokes equations on massively parallel computers. *Journal of Computational Physics* **229** (10), 3543–3572.

Hiemenz, K 1911 Die Grenzschicht an einem in den gleichförmigen Flüssigkeitsstrom eingetauchten geraden Kreiszylinder. *Dinglers Polytechnisches Journal* **326** (21-26), 321–324,344–348,357–362,372–376,391–393,407–410.

Hosseini, S M, Tempelmann, D, Hanifi, A & Henningson, D S 2013 Stabilization of a swept-wing boundary layer by distributed roughness elements. *Journal of Fluid Mechanics* **718**, R1.

Joslin, R D 1995 Direct Simulation of Evolution and Control of Three-Dimensional Instabilities in Attachment-Line Boundary Layers. *Journal of Fluid Mechanics* **291**, 369–392.

Landahl, M T 1980 A note on an algebraic instability of inviscid parallel shear flows. *Journal of Fluid Mechanics* **98** (02), 243–251.

Obrist, D, Henniger, R & Kleiser, L 2012 Subcritical spatial transition of swept Hiemenz flow. *International Journal of Heat and Fluid Flow* **35**, 61–67.

Obrist, D & Schmid, P J 2003 On the linear stability of swept attachment-line boundary layer flow. Part 2. Non-modal effects and receptivity. *Journal of Fluid Mechanics* **493**, 31–58.

Pfenninger, W 1977 Special Course on Concepts for Drag Reduction. Laminar Flow Control. Laminarization. *Tech. Rep.* AGARD Report No. 654. NATO-AGARD, Neuilly-sur-Seine.

Poll, D I A 1979 Transition in the Infinite Swept Attachment Line Boundary Layer. *Aeronautical Quarterly* **30** (Nov), 607–629.

Waleffe, F 1997 On a self-sustaining process in shear flows. *Physics of Fluids* **9** (4), 883.